Experimental assessment of time-reversed OFDM underwater communications

J. Gomes[a], A. Silva[b] and S. Jesus[b]

[a]ISR - Instituto Superior Tecnico, Av. Rovisco Pais, Torre Norte 7.22, 1049-001 Lisboa, Portugal
[b]ISR, Universidade do Algarve, PT-8005-139 Faro, Portugal
jpg@isr.ist.utl.pt

OFDM communication has recently been demonstrated in underwater channels at rates of $10-30$ kbps. This is a popular modulation in radio communications due to its spectral flexibility and the simplicity of FFT-based transmitters/receivers. Despite widespread interest, experimental data on the performance of underwater OFDM are still scarce. This work aims to contribute to a better understanding of the potential of this technique by examining results from the UAB'07 experiment, which was conducted in Norway, in September 2007. Modulated data were transmitted in a fjord using several formats with bandwidths of 1.5 and 4.5 kHz, and recorded at a range of about 800 m in a 16-hydrophone array. Significant multipath was observed over a period of at least 30 ms, which would call for a large OFDM prefix and hence drastically reduce the data rate. Passive time reversal is used here as a computationally inexpensive preprocessing scheme to shorten the effective channel length to less than 10 ms, so that moderate guard intervals can be used with a conventional OFDM receiver architecture. The same marker signals used for packet synchronization and Doppler compensation are reused as channel probes for passive time reversal, so the latter entails no loss in efficiency.

1 Introduction

Incoherent communication based on M-FSK modulation has been widely used in medium-speed underwater data links due to its resilience to multipath [1]. Coherent multicarrier modulation, on the other hand, has received less attention [2], which contrasts sharply with the large body of work on this subject in wireline and wireless radio communications, where orthogonal frequency-division multiplexing (OFDM) is one of the preferred ways of approaching capacity in frequency-selective channels. This discrepancy may be attributed to the perception that many off-vertical underwater channels are too complex and dynamic for the subtle orthogonality of carriers to be ensured reliably.

Although single-carrier modulation and equalization-based reception remains the technique of choice in bandwidth-efficient underwater communications, recently published experimental results have demonstrated successful OFDM communication in underwater channels [3, 4, 5]. In [3] data rates on the order of 20 kbps were attained in an experiment where channel impulse responses were relatively short, with an effective length of less than 5 ms. A data set from the same experiment was used [4].

This work presents results from the UAB'07 experiment, which was conducted in Norway, in September 2007. Modulated data were transmitted in a fjord using several formats with bandwidths of 1.5 and 4.5 kHz, and recorded at a range of about 800 m in a 16-hydrophone array. Significant multipath was observed over a period of at least 30 ms, which would call for a large OFDM prefix and hence drastically reduce the data rate. Channel conditions such as these are more likely to be encountered in practice than the short responses reported in [3, 4, 5]. Passive time reversal is used as a computationally inexpensive preprocessing scheme to shorten the effective channel length to less than 10 ms, so that moderate guard intervals can be used with a conventional OFDM receiver architecture [6].

Active time reversal is a wave backpropagation technique that takes advantage of the reciprocity of linear wave propagation to concentrate signals at desired points in a waveguide with little knowledge about the medium properties. In communications applications this may be achieved by transmitting a channel probe from the intended focal spot to an array of transducers that sample the incoming pressure field. These signals are then reversed in time, convolved with a single desired information waveform, and the resulting signals retransmitted, creating a replica field that converges on the original source location and approximately undoes the effects of multipath. Passive time reversal [7] is conceptually similar, yet both the probe and message are sequentially sent from the source, so the array only operates in receive mode. Focusing is performed synthetically at the array by convolving the time-reversed distorted probes with received data packets.

In the proposed approach the same marker signals used for OFDM packet synchronization and Doppler compensation are reused as channel probes for passive time reversal, so the latter entails no loss in efficiency. The performance of time-reversed OFDM is compared with that of single-carrier QPSK modulation using either time reversal or multichannel equalization at the receiver.

2 Passive Time Reversal of Communication Waveforms

A complex representation in terms of baseband equivalent signals (i.e., complex envelopes) is adopted here for the real passband waveforms that are transmitted and received across the channel. Time reversal of bandpass signals should then be replaced by time reversal and conjugation of complex envelopes.

In passive time reversal a channel probe $p(t)$ and an information signal $x(t)$ are sequentially sent from the same spatial location to an array (passive time-reversal mirror) with M hydrophones. In the absence of noise, the received signals at the m-th mirror transducer are obtained by convolving these waveforms with the medium impulse response $g_m(t)$

$$h_m(t) = r(t) * g_m(t)\,, \qquad r(t) \triangleq p(t) * p^*(-t)\,, \tag{1}$$

$$y_m(t) = x(t) * g_m(t)\,. \tag{2}$$

In (1) the definition of the distorted probe $h_m(t)$ already accounts for pulse compression at the receiver by crosscorrelating the received probe with $p^*(-t)$. For example, by choosing $p(t)$ as an LFM signal that sweeps across the bandwidth of $x(t)$, denoted by W_x, the crosscorrelation $r(t)$ will behave as an impulse over that band and $h_m(t)$ will suitably approximate the channel response $g_m(t)$.

The output of a passive mirror is obtained by convolving each received packet with the time-reversed probe,

and summing over all sensors

$$z(t) = \sum_{m=1}^{M} h_m^*(-t) * y_m(t) = r(t) * \gamma(t) * x(t)\,, \quad (3)$$

$$\gamma(t) \triangleq \sum_{m=1}^{M} g_m^*(-t) * g_m(t)\,. \quad (4)$$

The time reversal property ensures that the sum of medium autocorrelation functions, $\gamma(t)$, is nearly constant over W_x for a sufficiently long and dense mirror. If the same holds true for the spectrum of $r(t)$, as assumed above, then in the frequency domain

$$Z(\omega) = R(\omega)\Gamma(\omega)X(\omega) \approx CX(\omega) \quad (5)$$

for constant C, and $z(t)$ is a scaled replica of the undistorted packet $x(t)$. A practical mirror will not completely cancel the multipath distortion, but it may mitigate it to a point where conventional demodulation of OFDM signals becomes possible.

2.1 Doppler Preprocessing

In the presence of Doppler a nominal transmitted passband signal around ω_c, $\tilde{x}(t) = \mathrm{Re}\{x(t)e^{j\omega_c t}\}$, is perceived as

$$\tilde{x}((1+\beta)t) = \mathrm{Re}\{x((1+\beta)t)e^{j\omega_c \beta t}e^{j\omega_c t}\}\,, \quad (6)$$

where β is the time compression/dilation factor. This does not change the focusing properties of time reversal, but temporal scaling must be accounted for at the receiver when demodulating the digital message. A Doppler-compensated received signal is generated from $y_m(t)$ as

$$y'_m(t) = y_m\left(\frac{t}{1+\beta}\right) e^{-j\omega_c \frac{\beta t}{1+\beta}}\,, \quad (7)$$

and used in all subsequent processing. The same holds for channel probes. As shown in [8], this has negligible impact on the performance of time reversal.

Markers (LFM sweeps) are inserted at the beginning and end of each packet and detected by crosscorrelation at the mirror, so that β is readily computed by comparing the actual elapsed period with the nominal one [9]. The same markers are reused as channel probes for time reversal according to (1), as they span the full signal bandwidth.

3 OFDM Model and Processing

The OFDM signal format and receiver algorithms are similar to those reported in [3]. The signal generated at the focal spot comprises K subcarriers

$$x(t) = \sum_{k=0}^{K-1} \sum_{l} a_k(l) f_k(t - lT_b)\,, \quad (8)$$

where $a_k(l)$ denotes a point from the k-th subcarrier complex constellation in the l-th OFDM symbol interval, $f_k(t)$ is the corresponding pulse shape, and T_b is the OFDM symbol duration including any prefix/postfix. The pulses $f_k(t)$ are generated by exponential modulation from a single rectangular prototype of length T, $\Pi(t/T)$, as

$$f_k(t) = e^{j\frac{2\pi k}{T}t}\Pi\left(\frac{t}{T}\right)\,, \quad \Pi(t) \triangleq \begin{cases} 1\,, & 0 \le t < 1 \\ 0\,, & \text{otherwise.} \end{cases} \quad (9)$$

The guard interval is denoted by T_g, such that $T_b = T + T_g$. In line with [3], the model (9) corresponds to zero-padded (ZP) OFDM, which is known to raise fewer channel identifiability issues than the more conventional approach based on cyclic prefixes (CP). For the sake of simplicity, however, the receiver algorithms that were used in this work do not take advantage of this and synthetically emulate CP-OFDM by overlap-add prior to FFT processing.

An OFDM packet comprises N OFDM symbols, each occupying a bandwidth $W = K/T$. The complex values a_k used for the K subcarriers are selected as follows:

- $a_k = 0$ in K_g guard subcarriers allocated at the upper and lower band edges. These account for the nonzero rolloff of practical front-end bandpass filters, which may induce strong aliasing distortion when the received OFDM signal is sampled at the critical rate $f_s = K/T$ for FFT demodulation.
- $a_k = 0$ in K_n null subcarriers used for residual Doppler estimation.
- a_k known in K_p pilot carriers used for channel estimation. Preferably, these should be evenly spread over the signal bandwidth.
- Regular information symbols in the remaining K_a active carriers.

From this partitioning $K = K_g + K_n + K_p + K_a$.

3.1 Demodulation Algorithms

After Doppler preprocessing as described in Sec. 2.1 and passive time reversal, a single-channel signal $z(t)$ is obtained. This is sampled at the rate K/T, overlap-added by shifting each trailing guard interval to the start of its OFDM symbol, and a number of steps, given below, are then followed to retrieve the information sequence from the resulting discrete-time OFDM waveform $z(n)$. Each OFDM symbol is represented by a set of K samples covering the active interval of length T where $\Pi(t/T) = 1$ in (9), and processed independently from the remaining symbols in the packet. The description is brief, and the reader is referred to [3] for further details.

3.1.1 Residual Doppler Estimation

Even after Doppler scaling the signal may still exhibit a narrowband Doppler shift, i.e., the baseband OFDM signal is multiplied by an exponential term $e^{j\omega_d t}$ that degrades the orthogonality of carriers and creates intercarrier interference (ICI). An appropriate value for ω_d is found by grid search, minimizing the spillover of energy into the set of null subcarriers. Specifically, for each candidate ω_d on the grid the compensated signal

$z'(n) = e^{-j\omega_d n} z(n)$ is formed, its FFT is taken, and the cost function is evaluated as the squared sum of coefficients at the null subcarrier indices. As the number of null subcarriers, K_n, is much smaller than K, it may be more efficient to compute the DFT values for individual null carrier frequencies, rather than taking the full FFT.

3.1.2 Channel Estimation and Frequency-Domain Equalization

Using K_p pilot symbols allows up to K_p impulse response coefficients to be estimated by solving a standard linear least-squares problem. Let $Z(p_i)$ denote the FFT of $z(n)$ at one of the pilot carrier indices $p_1, \ldots, p_{K_p}$. Then the parameters of an N_h-order frequency response

$$H(k) = \sum_{n=0}^{N_h} h_l e^{-j\frac{2\pi k}{K} n} \tag{10}$$

are obtained from

$$\min_{h_0,\ldots,h_{N_h}} \sum_{i=1}^{K_p} \left| Z(p_i) - a_{p_i} H(p_i) \right|^2 \tag{11}$$

when $N_h < K_p$. Unknown symbols in active subcarriers are estimated by frequency-domain equalization using the interpolated values of (10),

$$\hat{a}_k = \frac{Z(k)}{H(k)} \,. \tag{12}$$

3.1.3 Outer coding

Practical applications of OFDM almost always use some form of outer coding and interleaving as forward error correction to improve the robustness against deep channel fades in some of the subcarriers. In the UAB'07 trial the same coding/interleaving steps described below are also applied to single-carrier QPSK packets.

Transmitter: The raw bit stream at the transmitter is first convolutionally encoded using a popular rate 1/2 code with constraint length 7, maximum free distance (10), and octal generators $(133, 171)$ [10]. The code is punctured by eliminating 1 out of 3 bits, thus increasing the rate to 3/4. The coded bits are then randomly interleaved and partitioned into subblocks to be mapped into OFDM symbols.

Receiver: As the subblocks of coded bits from an OFDM packet are demodulated at the receiver, they are randomly deinterleaved and the Viterbi algorithm is then used to retrieve the raw bit stream. To limit the decoding latency, the latter operates with a traceback length equal to 35, or 5 times the code constraint length.

4 The UAB'07 Sea Trial

The Underwater Acoustic Barriers (UAB) sea trial was carried out in Norway during the first two weeks of September 2007. The OFDM experiment reported here was conducted in Trondheim fjord on September 5. The transmitter was suspended from a fixed platform 10 m from shore, at a depth of about 5 m. The receiver was a vertical array with 16 uniformly-spaced hydrophones from 6 m to 66 m depth, suspended from a drifting Acoustic Oceanographic Buoy (AOB) developed at the University of Algarve. The communication range was approximately 800 m, the bottom depth gradually increasing from 10 m at the transmitter to about 100 m at the receiver location.

Several modulation formats were transmitted with bandwidths of 1.5 kHz and 4.5 kHz, and carrier frequency 5.5 kHz. Tabs. 2 and 1 summarize the parameters for OFDM and single-carrier QPSK packets. In OFDM packets $K_g \approx 0.15K$ guard carriers are set aside at the lower and upper band edges. Bandpass front-end filtering at the receiver can then be easily accomplished in practice using a raised-cosine filter with 15% rolloff.

Each packet listed in Tabs. 2 and 1 is flanked by a pair of start/stop LFM markers to be detected by cross-correlation for packet synchronization and Doppler compensation (Sec. 2.1). Each LFM marker sweeps across the band 5.5 ± 2.25 kHz in 20 ms, and is preceded/succeeded by a 50 ms silent period for transient die out.

Table 1: QPSK signal parameters

Packet type	Q1	Q2
Bandwidth [kHz]	1.5	4.5
Pulse shape	Root raised-cosine	
Rolloff [%]	50	
Symbol interval T_b [ms]	1	0.3
Symbol rate [kbaud]	1	3
Number of symbols N	3×10^3	9×10^3
Packet duration [s]	3	
Constellation	QPSK	

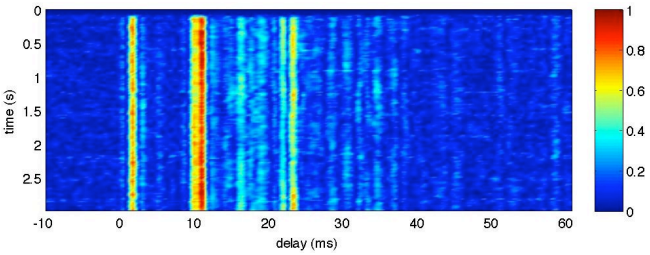

Figure 1: Evolution of the amplitude-normalized estimated channel response at depth 22 m (hydrophone #5) for a Q1 packet (1 kbaud). Doppler precompensation was performed according to Sec. 2.1

5 Experimental Results

Channel responses: Fig. 1 shows the evolution of the estimated impulse response at depth 22 m (hydrophone #5) in a Q1 packet. Doppler precompensation was performed according to Sec. 2.1, stabilizing the arrival structure in both magnitude and delay. Three main arrivals are visible, and significant multipath energy is observed over a period of about 30 ms. These results were obtained by running the exponentially windowed RLS algorithm ($\lambda = 0.98$) on a bank of identification filters

Table 2: OFDM signal parameters

Packet type	O1	O2	O3	O4	O5	O6
Bandwidth [kHz]	1.5	1.5	1.5	4.5	4.5	4.5
Total carriers K	64	128	256	128	256	512
Null carriers K_n	3	5	10	5	10	20
Guard carriers K_g	10	20	40	20	40	78
Symbol interval T_b [ms]	42.7	85.3	170.7	28.4	56.9	113.8
Guard interval T_g [ms]	30					
Number of symbols N	40	30	15	60	40	20
Packet duration [s]	2.91	3.46	3.01	3.51	3.48	2.88
Constellation	QPSK					

Table 3: Parameters and performance for multichannel equalization of QPSK packets

Packet type	Q1	Q2
Equalizer type	DFE	
Adaptation algorithm	QR-RLS	
Forgetting factor	0.995	
Number of hydrophones	8 (#1,#3, ..., #15)	
Oversampling factor	2	
Forward filter order	$(13, 4) \times 16$	$(9, 2) \times 16$
Feedback filter order	40	60
MSE (dB)	-24.3	-17.8
Symbol errors	0	0
Bit errors	0	0

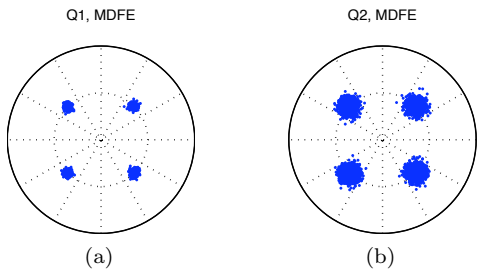

Figure 2: Output constellations for multichannel equalization of QPSK data (a) Q1 packet, 1 kbaud (b) Q2 packet, 3 kbaud

with 61 causal and 10 anticausal coefficients (abbreviated as $(61, 10)$), as described in [8].

Equalization of QPSK packets : To benchmark the performance of OFDM, results are presented for conventional equalization-based demodulation of single-carrier packets. Fig. 2 shows the output constellation for Q1 and Q2 packets using a multichannel DFE whose parameters are given in Tab. 3. For 8 hydrophones and 2-oversampling the forward filter operates on $8 \times 2 = 16$ input sample streams at symbol rate. The notation used in Tab. 3 for forward filter order indicates the number of causal and anticausal coefficients that were allocated to each of those streams [8]. Equalizer orders were manually chosen for best performance, and training was based on the initial 10% packet symbols. Tab. 3 also lists steady-state MSE values, the number of raw symbol errors, and the number of bit errors after Viterbi decoding.

Table 4: Parameters and performance for time reversal and single-channel post-equalization of QPSK packets

Packet type	Q1	Q2
Equalizer type	DFE	
Adaptation algorithm	QR-RLS	
Forgetting factor	0.995	
Oversampling factor	2	
Forward filter order	$(11, 10) \times 2$	$(21, 20) \times 2$
Feedback filter order	1	1
MSE (dB)	-15.4	-15.4
Symbol errors	0	0
Bit errors	0	0

Tab. 4 provides similar data for passive time reversal, followed by single channel equalization. Residual MSE values are larger than those of Tab. 3, particularly for Q1 packets, due to long-term residual intersymbol interference from the convolutions in (3), but the choice of suitable equalizer parameters is simpler. Fig. 3 shows estimated impulse responses for a Q2 packet (3 kbaud) observed at the outputs of hydrophone #5 and the passive time-reversal mirror. Compression of the impulse response in Fig. 3b to less than 10 ms suggests that time reversal may indeed be useful as an enabling technology for demodulating OFDM over channels with severe delay dispersion. This is verified next.

OFDM demodulation: The proposed approach for time-reversed OFDM demodulation (TR-OFDM) is compared with maximal ratio combining (MRC-OFDM) [3], where OFDM processing as described in Sec. 3.1 is performed in parallel over a set of hydrophones to yield pairs of observations/channel estimates $(Z_m(k), H_m(k))$, $m = 1, \ldots, M$, from which $\hat{a}_k$ is obtained by least-squares fitting to $\sum_m |Z_m(k) - a_k H_m(k)|^2$ instead of (12). Tab. 5 lists the performance metrics for both approaches when 1 out of 4 subcarriers (excluding guard and null carriers) is used for training.

6 Discussion and Conclusion

The results of Tab. 5 show that the MRC-OFDM approach of [3] tends to perform poorly in the UAB'07 data set. Given the extent of observed channel impulse responses, which are at least as long as OFDM guard

Table 5: Performance of MRC-OFDM and TR-OFDM using 1 out of 4 subcarriers for training

	MRC-OFDM						TR-OFDM					
Packet type	O1	O2	O3	O4	O5	O6	O1	O2	O3	O4	O5	O6
MSE (dB)	−1.0	−4.1	−9.3	−1.1	−1.8	−5.4	−3.3	−5.7	−7.1	3.2	−3.2	−7.6
Symbol errors	894	312	14	2124	2527	403	105	22	17	483	266	55
Bit errors	1847	1473	0	5448	7278	1265	343	3	9	1955	665	25

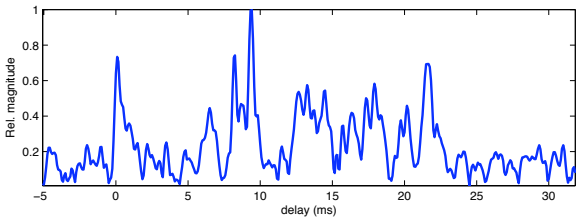

(a)

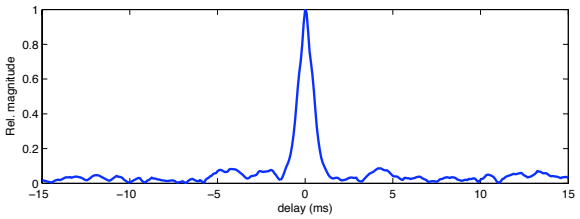

(b)

Figure 3: Amplitude-normalized estimated channel responses for a Q2 packet (a) Received signal at hydrophone #5 (b) Passive mirror output

intervals, the observations/channel estimates obtained at each hydrophone are so unreliable that subsequent multichannel combining fails. TR-OFDM performs significantly better, as the equivalent time-reversed channel impulse response is both shorter and more predictable (sinc-like). Moreover, TR-OFDM is computationally simpler because OFDM demodulation is performed on a single signal, whereas in MRC-OFDM it is done for each sensor in the receiver array.

For similar spectral efficiencies in QPSK and OFDM packets, best performance was obtained in the former using equalization. However, it should be stressed that selecting *a priori* an appropriate set of equalizer parameters is not trivial (but simpler after time reversal). These results indicate that enhanced channel estimation methods are a relevant topic for future work in TR-OFDM. Alternative strategies to frequency-domain equalization using (12) should also be examined.

Residual Doppler estimation also has a major impact on performance and should be improved. When the number of null carriers is too low the method of Sec. 3.1.1 yields Doppler estimates with somewhat erratic variation between successive OFDM symbols, suggesting that these values are unreliable and significant ICI may exist. This would explain the poor results that were obtained in Tab. 5 for O1 packets, where there are only 3 null carriers.

In conclusion, one could say that the results for TR-OFDM are encouraging, but improvements are needed before it can be considered as an alternative to single-carrier transmission in severely dispersive channels.

Acknowledgments

This work was supported by Fundação para a Ciência e a Tecnologia through project PTDC/EEA-TEL/71263/2006 and ISR/IST plurianual funding.

References

[1] D. B. Kilfoyle and A. B. Baggeroer, "The state of the art in underwater acoustic telemetry," *IEEE J. Oceanic Eng.*, vol. 25, no. 1, pp. 4–27, Jan. 2000.

[2] W. K. Lam, R. F. Ormondroyd, and J. J. Davies, "A frequency domain adaptive coded decision-feedback equalizer for a broadband UWA COFDM system," in *Proc. MTS/IEEE OCEANS'98*, vol. 2, Nice, France, Sept. 1998.

[3] B. Li, S. Zhou, M. Stojanovic, and L. Freitag, "Pilot-tone based ZP-OFDM demodulation for an underwater acoustic channel," in *Proc. MTS/IEEE OCEANS'06*, Boston, USA, Sept. 2006.

[4] M. Stojanovic, "Low complexity OFDM detector for underwater acoustic channels," in *Proc. MTS/IEEE OCEANS'06*, Boston, USA, Sept. 2006.

[5] B. Li, S. Zhou, M. Stojanovic, L. Freitag, J. Huang, and P. Willett, "MIMO-OFDM over an underwater acoustic channel," in *Proc. MTS/IEEE OCEANS'07*, Vancouver, Canada, Sept. 2007.

[6] J. Gomes and V. Barroso, "Time-reversed OFDM communication in underwater channels," in *Proc. IEEE SPAWC'04*, Lisboa, Portugal, Jul. 2004.

[7] D. R. Dowling, "Acoustic pulse compression using passive phase-conjugate processing," *J. Acoust. Soc. America*, vol. 95, no. 3, pp. 1450–1458, Mar. 1994.

[8] J. Gomes, A. Silva, and S. Jesus, "Adaptive spatial combining for passive time-reversed communications," *Accepted in J. Acoust. Soc. America*, 2008.

[9] B. S. Sharif, J. Neasham, O. R. Hinton, and A. E. Adams, "A computationally efficient doppler compensation system for underwater acoustic communications," *IEEE J. Oceanic Eng.*, vol. 25, no. 1, pp. 52–61, Jan. 2000.

[10] J. G. Proakis, *Digital Communications*, 4th ed. McGraw-Hill, 2000.